Enhancing the out-of-plane performance of masonry walls using engineered cementitious composite

S. Pourfalah*,

B. Suryanto,

D. Cotsovos

Heriot Watt University,

School of Energy, Geoscience, Infrastructure and Society,

Edinburgh, EH14 4AS, Scotland,

U.K.

* Corresponding Author

E-mail: sp315@hw.ac.uk

Tel: +44 (0)7719796299

Abstract: A novel method for enhancing the out-of-plane behaviour of masonry infill walls is proposed herein. The technique involves the use of a thin layer of engineered cementitious composite (ECC) which is fully or partially bonded onto the face of masonry walls. To investigate the feasibility of this technique, the present study focuses on investigating the behaviour of a series of beam-like masonry specimens with and without ECC retrofitting subjected to four-point bending, with the load applied monotonically to failure at rates of 1 mm/min and 200 mm/min. The results show that the ECC-retrofitted specimens exhibited a significant enhancement in the out-of-plane performance in terms of strength, stiffness and ductility as compared to that of the un-strengthened specimens. It is shown that specimens with a partially bonded ECC layer performed better than their counterparts having a fully bonded ECC layer. Partial de-bonding is shown to allow the ECC to achieve its full ductility potential. The results also show that specimens subjected to higher loading rates exhibit higher load-carrying capacity and stiffness but lower ductility.

Keywords: engineered cementitious composite, masonry, infill walls, out-of-plane behaviour, strengthening, bond strength, cracking, failure mode, ductility, flexural testing. loading rate.

1. INTRODUCTION

The contribution of infill masonry walls to the overall behaviour of frame structures has been acknowledged through numerous published experimental and numerical investigations carried out to date [1-3]. Such walls can be subjected to a range of in-plane and out-of-plane actions (e.g. wind, earthquakes, impact explosion and blast loads). Infill walls are particularly vulnerable to the application of loads in the out-of-plane direction that can result in them sustaining cracking which can lead to their full or partial collapse [4, 5]. After sustaining a certain level of damage, an infill wall can no longer contribute to the response of the frame structure with its in-plane stiffness. This can potentially have a detrimental effect on the overall response of the frame structures, resulting in often unpredictable forms of failure or even collapse [6]. In an attempt to safeguard structural integrity and resilience, FEMA-306 [7] recommends the calculation of the load-carrying capacity of masonry infill walls associated with an out-of-plane response under seismic excitation whereas EC8 [8] specifically states that appropriate measures should be taken in order to prohibit partial or total out-of-plane collapse of slender masonry infill walls.

The out-of-plane behaviour of masonry walls has been experimentally and numerically investigated under static and dynamic (ranging from earthquake to impact and blast) loads [4, 5]. These studies reveal that the out-of-plane response of the infill walls is dependent on their geometry (e.g. slenderness) and the mechanical properties of the materials used for their construction however, it is usually characterized by limited load-carrying capacity and ductility [6]. Furthermore, it is interesting to note that the damage sustained by masonry infill walls during earthquakes have been identified as the primary cause of injuries and fatalities [9] whereas the associated repair costs represent a large portion of the total rehabilitation costs of frame structures.

Based on the above, it is essential that masonry walls are designed to safely undertake loads applied in the out-of-plane direction in order to ensure public safety and safeguard structural integrity and resilience. Several retrofitting methods have been developed and employed in practice for enhancing the out-of-plane performance of infill masonry walls in terms of load-carrying capacity and deformability. Additional reinforcement, either in the form of a steel mesh embedded within a cement/concrete render [10-14] or, in the form of metal or fibre reinforced polymer (FRP) layers or strips are often attached onto the wall surface [15-17] in order to form a composite member characterised by improved strength and stiffness. While these methods improve certain characteristics of the out-of-plane behaviour of masonry infill walls, their application can often be intrusive and characterized by series of problems associated with the increase of the mass of the building, the high application costs, problems associated with the level of bond (developing along the interface of the original masonry wall and the newly formed layer) as well as the brittle forms of failure often exhibited which are accompanied by the generation of fragments or debris [17-19]. In an attempt to address these problems and enhance the overall behaviour of infill masonry walls, present work employs a thin layer of engineered cementitious composite (ECC) which is fully or partially bonded onto the face of the masonry wall acting in tension (opposite to the face on which the out-of-plane action is applied).

The present experimental study sets out to investigate the potential benefits stemming from the use of ECC on the out-of-plane behaviour of infill masonry walls. ECC exhibits ductile, strain-hardening behaviour under uniaxial tension, typically characterised by a high strain capacity (a few %) and toughness [20]. This is mainly attributed to the ability of the material to form multiple fine cracks, with average crack widths less than 100 microns. Studies have shown that the tensile behaviour of ECC is, however, sensitive to strain rate [21, 22]. When subjected to increasing rates of tensile loading, the ECC material behaviour is shown to

exhibit: (i) a reduction in ductility accompanied by an increase in apparent strength, when compared to the response under static loading; and (b) the development of more localised (clustered) cracking, with larger crack widths. When used with masonry elements, existing studies have shown that the use of ECC layers can improve the out-of-plane behaviour of masonry wall specimens [23-25]. The application of a thin fully-bonded ECC layer on the surface of masonry walls has been found to enhance the out-of-plane behaviour of masonry wall specimens, including the load-carrying capacity, stiffness and ductility [24-26]. This is because the strengthened specimens are able to absorb more effectively the energy introduced during loading. However, it is important to point out that in all relevant experimental studies carried out to date, the ECC layer exhibits localised (instead of distributed) cracking, concentrated in the joint regions between consecutive bricks. This suggests that the full potential of ECC is not achieved prior to failure due to the interaction between the masonry and the ECC layer [23-25].

The present study attempts to prevent the development of localised damage (cracking) to the ECC retrofitting layer and improve the behaviour of the ECC-retrofitted masonry walls when subjected to out-of-plane loads by partially bonding the ECC layer to the surface of the masonry wall. Partial bonding of an ECC repair layer onto a simply supported concrete beam substrate was found to be beneficial, allowing a kink-crack trapping mechanism to develop which produces distributed micro-crack formation along the un-bonded region [26]. This idea is presently applied for the case of ECC-retrofitted masonry infill walls in order to improve their out-of-plane behaviour. Initially, a series of tests were carried out to establish the behaviour of the individual materials used for the construction of the masonry specimens as well as their interactions. This was then followed by a second series of tests investigating the behaviour of the retrofitted masonry beam-like specimens (essentially consisting of a stack of bricks connected with mortar joints in between) subjected to four-point bending tests. The

load was applied monotonically to failure under two different rates of loading: 1mm/min and 200 mm/min. The subject specimens represent a simplistic representation of a vertical strip of a masonry infill wall which can be subjected to loads with different characteristics (associated with their distribution, their time history, their loading rate and intensities). The aim of the four-point loading tests is to verify in principle the ability of the proposed strengthening methods to enhance structural behaviour. The experimental study was also complemented by a numerical investigation, based on the use of nonlinear finite element analysis (NLFEA), the predictions of which confirm the main conclusions drawn from the analysis of the test data while at the same time providing more detailed insights into the mechanics underlying the behaviour of the test specimens to failure.

2. EXPERIMENTAL PROGRAM

A series of tests were carried out in order to study experimentally (a) the behaviour of the materials used and their interactions; and (b) the potential benefits stemming from the use of fully or partially bonded ECC layers on the out-of-plane performance of masonry beam-like specimens. A summary of the tests conducted is provided in Table 1.

Table 1. Summary of tests conducted.

Type of test	Specimen	Loading rate	ID
Compression tests	Brick unit	200 kN/min	CB
	Mortar prism/cylinder		CM
	Brickwork prism	150 kN/min	CBM
Crossed-brick tensile tests	Brick/mortar couplet	1 mm/min	TBM
Triplet shear tests	Brick/mortar triplet	0.2 mm/min	SBM
	Brick/ECC triplet		SBE
Direct tensile tests	Dog-bone shape ECC	1 mm/min	ST
		400 mm/min	ET
Flexural tests	Non- retrofitted masonry beams	1 mm/min	SN
		200 mm/min	EN
	Prisms with a fully bonded ECC layer	1 mm/min	SF
		200 mm/min	EF
	Prisms with a partially bonded ECC layer	1 mm/min	SP
		200 mm/min	EP

144 **2.1 Experiments carried out to study material or interface behavior**

145 A brief presentation of the specimens and test setup employed for establishing material and
146 interface behaviour is provided in this section.

147 **Testing of brick units and mortar specimens under uniaxial compression:** Class B
148 Engineering solid clay bricks (in accordance to BS EN 771-1 [27]) with dimensions of
149 210×102×65 mm (CB series) were tested under uniaxial compression according to ASTM
150 C67-14 [28]. These tests aimed at determining the average compressive strength and modulus
151 of elasticity of the brick units. Prior to testing, each brick unit was initially dried in an oven at
152 a temperature of 110ºC for 24 hours and was then cooled down at room temperature for 4
153 hours. Each brick was then capped on its upper and lower face with a 3mm thick layer of fast
154 hardening high-strength cement. After the mortar sufficiently hardened, each brick was
155 positioned in a 3000kN Avery-Denison testing machine, with the bed surface (100×102 mm)
156 aligned with the direction of loading. Two Linear Variable Displacement Transducers
157 (LVDTs) were placed at each side of the brick to measure the relative displacements of the
158 top and bottom loading plates. The load was applied in the form of force increments (load-
159 control) at a rate of 200 kN/min.

160 The mortar used in this study comprised of one part of CEM I 52.5N Portland cement in
161 accordance to BS EN197-1 [29] and three parts (by mass) of fine dry silica sand (with an
162 average particle size of 120 μm). The water-to-cement ratio was fixed at 0.85 (by mass). The
163 specimens were de-molded 24 hours after casting before being cured for a period of 28 days.
164 They were then tested under uniaxial compression as in the case of the brick units.
165
166 **Crossed-brick couplet tests:** Five crossed-brick couplets (TBM series) were fabricated to
167 investigate the bond strength of the brick/mortar interface in accordance to ASTM C952-12
168 [30]. Prior to fabrication, all bricks were submerged in water for 24 hours. After drying off

their surface, crossed-brick couplet specimens with a 5mm thick mortar joint were fabricated (see Figure 1). They were then cured indoors under damp hessian cloth and plastic covers for 28 days. During testing, the upper brick of each specimen was supported at three locations using three M20 steel bolts which rested on the lower rigid steel platen of a 500kN Instron testing machine, as shown in Figure 1. A similar bolt arrangement was used to apply the load to the lower brick as shown in the same figure. Three 10mm steel ball bearings were placed in between the bolts and the upper loading platen, in order to minimize any eccentricity. The load was applied in the form of displacement increments at a rate of 1 mm/min.

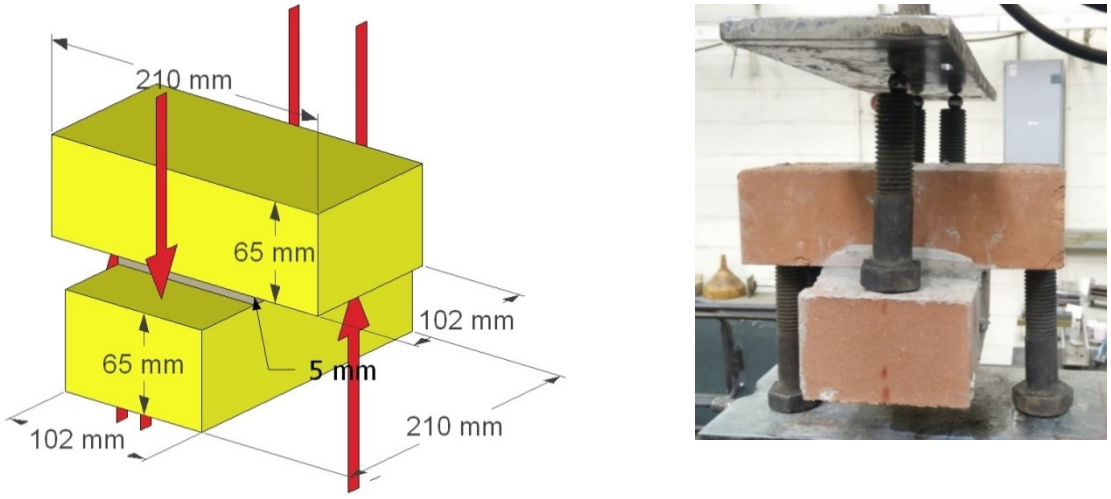

(a) (b)

Figure 1: Crossed-brick couplet tests (TBM series): (a) specimen dimensions, (b) test setup

Triplet brick test: Five brick/mortar triplets (SBM series) and four brick/ECC triplets (SBE series) were tested in accordance to BS EN 1052-3:2002 [31]. The brick/mortar triplets consisted of three bricks with two 5mm thick mortar layers (joints) in between (see Figure 2(a)) whereas the brick/ECC triplets consisted of three bricks with two 15mm thick ECC joints (see Figure 2(c)). After fabrication, all specimens were cured under damp hessian and plastic covers in the laboratory environment for 28 days. The specimens were then subjected to 4-point bending tests, as shown in Figure 2. The load was applied through two 10mm diameter steel loading rods which were positioned at a distance of approximately 14mm from

the edge of the middle brick. A 12mm thick steel plate with a surface of 65×100 mm was used to distribute the load over the top of the middle brick, with the outer two bricks supported on two 12mm thick steel plates. Each plate was in turn supported on a 10mm diameter steel bearing rod positioned 14mm from the edge of the joint (see Figures 2(b) and (d)). The tests were carried out using a 500kN Instron testing machine, with the crosshead (used for applying the load) moving at a speed of 0.2 mm/min. Two LVDTs were mounted on each side of the specimens to measure the deflection at mid-span (see Figures 2(b) and (d)).

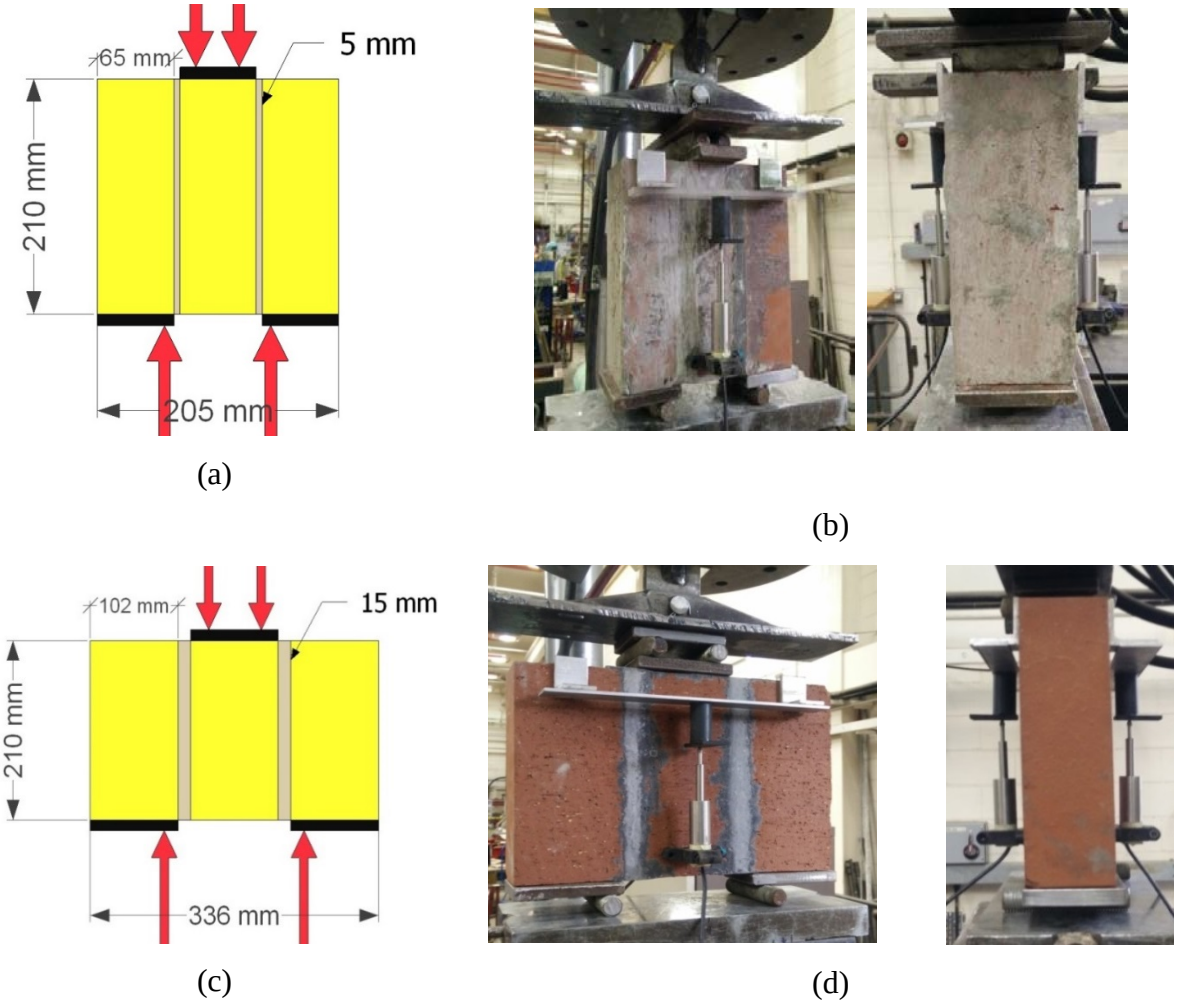

Figure 2: Triplet shear test: (a) dimensions of SBM specimen, (b) test setup for SBM specimens, (c) dimensions of SBE specimens, (d) test setup for SBE specimens

Uniaxial compression tests on masonry prisms: Five masonry prismatic specimens (CBM series) each comprising of four bricks and three 5mm thick mortar joints in between (see

Figure 3) were tested in compression in accordance to ASTM C1314-14 [32]. The testing arrangement is shown in Figure 3. After fabrication, the specimens were cured indoors under damp hessian and plastic cover in the laboratory environment for 28 days. Prior to testing, the top surface of each masonry prism was capped with a thin cement layer in accordance to ASTM C1552 [33]. The tests were then carried out using a 3000kN Avery-Denison testing machine, with the load being applied monotonically to failure at a loading rate of 150 kN/min. Two LVDTs were mounted at each side of the specimens at a gauge length of 210 mm (see Figure 3).

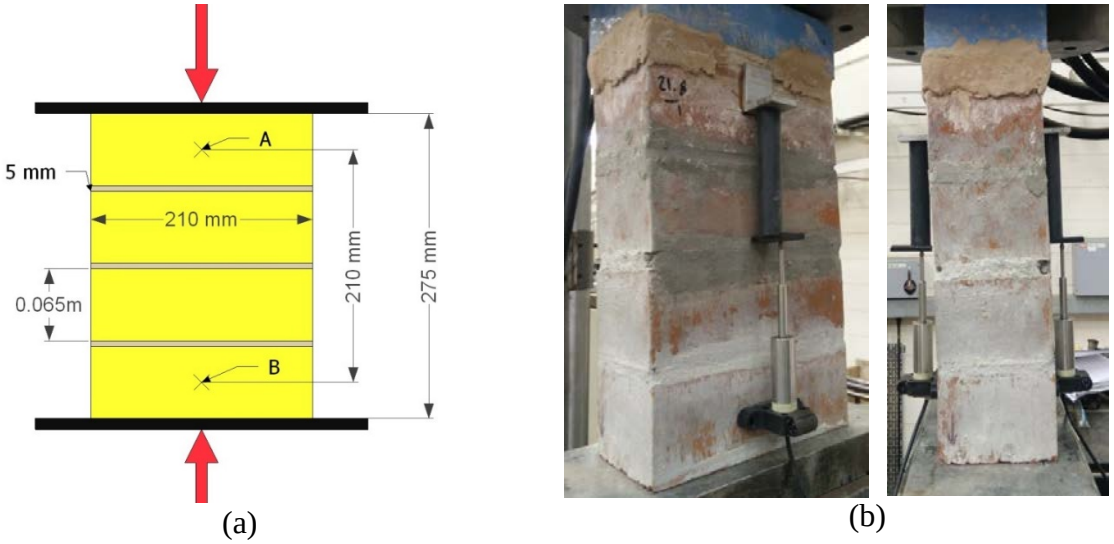

Figure 3: Brickwork compression test (CBM series): (a) dimensions of specimen, (b) test setup

Uniaxial tensile testing of ECC dog-bone specimens: Ten dog-bone shaped specimens with dimensions in accordance to JSCE (2008) [34] (see Figure 4a) were prepared to study the ECC material behaviour under uniaxial tensile loading. The ECC binder comprised of CEM I 52.5N Portland cement in accordance with BS EN197-1 [29] and fine fly-ash (Superpozz SV80, Scotash). These two components were mixed at fly-ash-to-cement ratio of 1.8 (by mass) and at water-to-binder ratio of 0.28. Fine silica sand with an average particle size of 120 μm was used as the filler at a sand-to-cement ratio of 0.6 (by mass), together with a polycarboxylate high-range water-reducing admixture (at a dosage rate of 1% by the cement

weight) and 12mm long polyvinyl alcohol (PVA) fibres (at a dosage of 2% by volume). The PVA fibres had an average diameter of 39μm and a tensile strength of 1600MPa. They came with a proprietary oiling agent coating to reduce the fiber/matrix chemical bond strength, thereby enabling the ECC to achieve its desired properties. After fabrication, the specimens were cured in water for 28 days. Direct tensile testing was performed using a 100kN Instron testing machine, with each dog-bone specimen initially clamped on both ends. It was then subjected to uniaxial tensile loading to failure; five specimens were tested at a loading rate of 1 mm/min (ST series) whereas five others at a rate of 400mm/min (ET series). LVDTs were mounted on each side of the dog-bone specimen to measure the elongation of the centre region throughout the loading process (see Figure 4(b)).

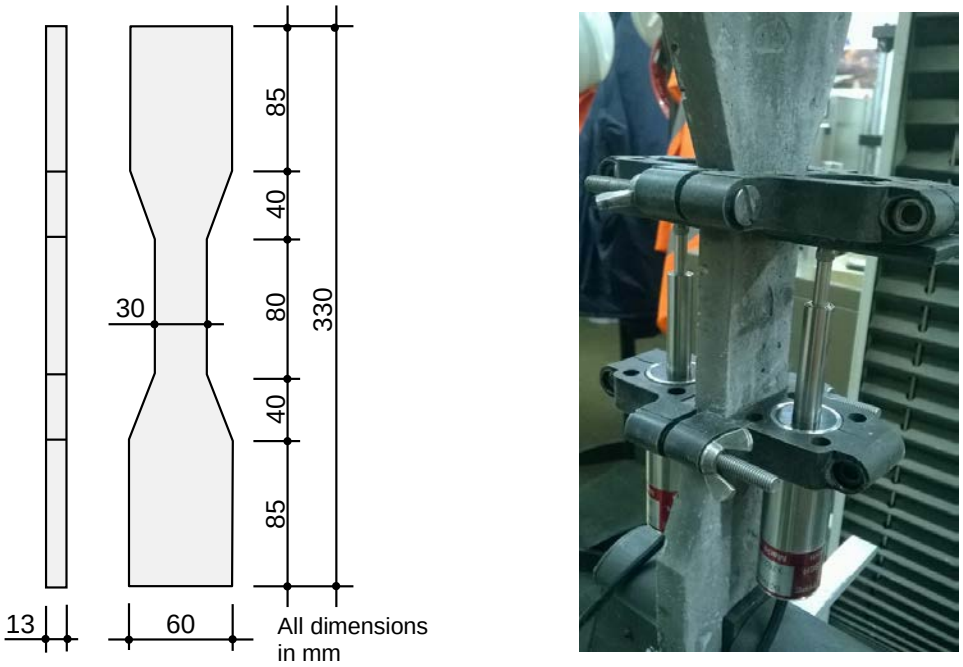

(a) (b)

Figure 4: Tensile testing of ECC dog-bone shaped samples: (a) schematic diagram; (b) sample during uniaxial tensile testing.

2.2 Masonry beam-like specimens

A total of fifteen beam-like masonry specimens were subjected to four-point bending tests.

Each specimen consisted of 10 bricks with 9 mortar joints in between. Four specimens were unstrengthened (no ECC layer was introduced to them), serving as a benchmark for the retrofitted specimens (see Figure 5(a)). Two of these specimens were tested at a loading rate of 1mm/min (SN series) and the remaining two at 200 mm/min (EN series). Six specimens were retrofitted with a 15mm thick layer of ECC fully-bonded to the bottom face of the beam-like specimens (see Figure 5(b)). Three of these specimens were tested at the rate of 1mm/min (SF series) and the other three at a rate of 200mm/min (EF series). The five remaining specimens were retrofitted with a 15mm thick layer of ECC partially-bonded to the bottom face of the beam (see Figure 5(c)), with the unbonded region extending over the 330 mm center region below the 4 middle bricks. Two of these specimens were tested at a loading rate of 1mm/min (SP series) and the remaining three were tested at a rate of 200mm/min (EP series). The dimensions of each masonry prismatic specimen was: (a) 720 (±20) mm in length, 210mm in width and 102mm in thickness in the case of the un-strengthened specimen (SN and EN series, see Figure 5(a)) and (ii) 720 (±20) mm in length, 210mm in width and 117mm in thickness for the case of the strengthened specimens (SF, SP, EF and EP series) (see Figures 5(b) and (c)).

Fabrication and curing process: The bricks were initially immersed in water for a period of 24 hours. After wiping the surface moisture with a dry cloth, the bricks were stacked vertically, with cement mortar used to form 5-10 mm thick joints in between (see Figure 6(a)). The mortar joints were made flush with the brick ends with the exception of the first two outer joints which were tooled concave on one face (approximately 5-10 mm deep), in order to provide an additional mechanical bond between the brick and the ECC layer (see Figures 6(b) and (c)). All specimens were covered with damp hessian and cured in the

laboratory for 14 days. This marked the completion of the fabrications process for the un-strengthened specimens (SN and EN series).

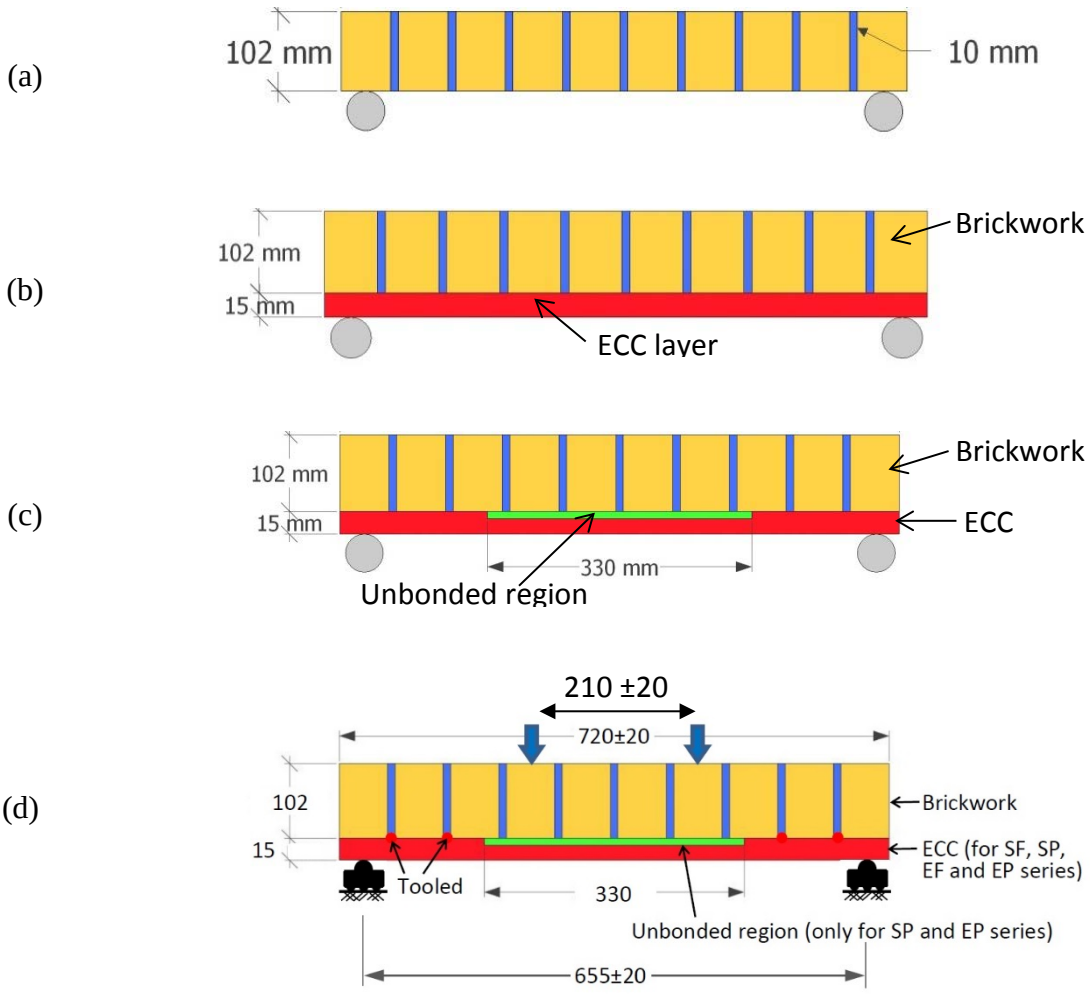

Figure 5: Schematic diagram of the four-point bending tests (dimensions in mm). (a) N series, (b) F series (c) P series (d). test setup

The specimens strengthened with an ECC layer (SP, SF, EP, EF series) were laid on a flat floor (see Figures 6(b) and (c)) and a timber frame was then constructed around the perimeter top surface of the specimens, forming a dike with internal dimensions of 740mm × 210mm × 15mm into which the ECC layer was cast. In the case of the specimens strengthened with a partially bonded ECC layer (SP and EP series), a duct-tape was fitted to the surface of the bricks along their middle third span (see Figure 6c) to minimize the interfacial bond between

the ECC layer and the masonry. Prior to casting the ECC, the surface of the masonry was wetted to minimize the absorption of water from the fresh ECC by the masonry and consequently minimize any influence this could potentially have on the material properties of the ECC layer. The ECC was produced using a 10-litre Hobart planetary motion mixer in batches of 7 litres. Immediately after mixing, the ECC was casted by pouring the fresh ECC from one end of the mold to the other end (see Figure 6(d)). The top surface was then troweled and tapped in places (see Figure 6(e)), in order to release the air bubbles. Finally, the top surface was covered with a plastic sheet (see Figure 6(f)). The timber formwork was removed after a day and the ECC was then cured under damp hessian and plastic sheeting for 28 days.

Experimental setup and instrumentation: The test setup used to perform the 4-point bending test is shown in Figure 7. Each specimen was supported on two rollers resting on a rigid steel base (see Figure 7(a)). The strengthened specimens (SF, SP, EF, and EP series) were positioned with the ECC layer being located on their bottom face (see Figure 7(b)). The load was applied through a custom-made spreader plate (see Figure 7(c)), allowing the two loading points to be adjusted (by ±40 mm) to account for small variations in the specimen length.

The reaction load was measured from a load cell incorporated in the Instron machine, whereas the mid-span vertical deflection was measured using two LVDTs located on each side of the specimen, which were mounted on a steel frame that was independently supported directly onto the rigid base (see Figures 7(b) and (e)). The LVDTs were connected to a data acquisition system which acquired data at a rate of 10 Hz.

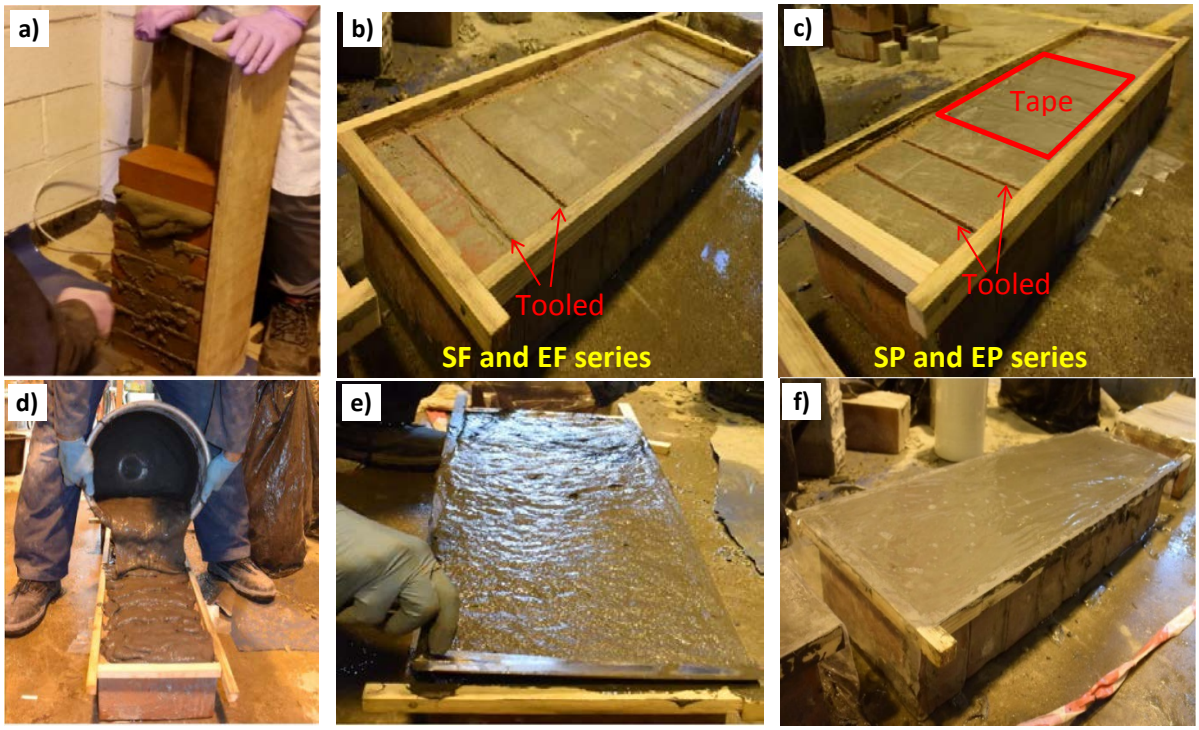

Figure 6: Fabrication process for the masonry beam-like specimens: (a) building the brickwork; (b) SF and EF series specimen showing the timber mould and groove at both ends; (c) SP and EP series specimen showing the duct tape, timber mould and groove at both ends; (d) ECC casting; (e) trowelling ECC surface; and (f) covering the top surface with plastic sheeting.

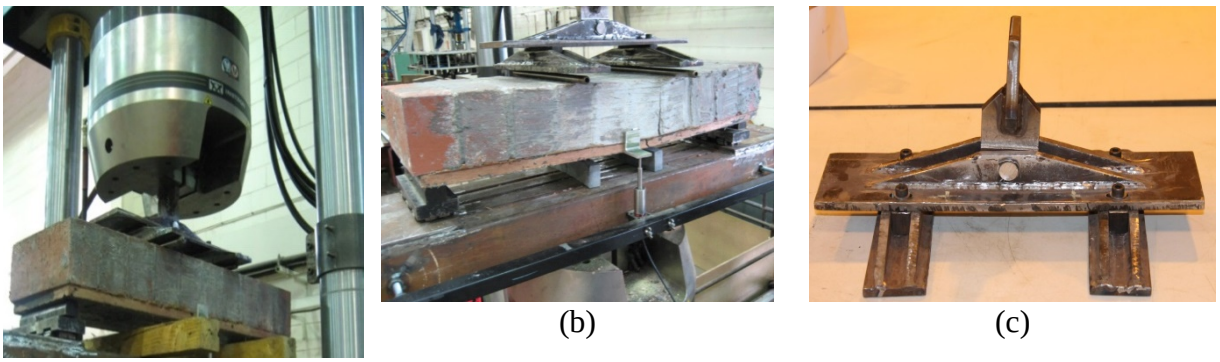

(b) (c)

(a)

(d) (e)

Figure 7. Four-point bending test setup a) Instron machine, b) Loading rig, supports and LVDT positions, c) loading rig d) support e) LVDT holder

3.0 RESULTS OBTAINED FROM THE MATERIAL TESTS

Compression tests: A summary of the results obtained from the compression tests carried out on the brick units and the mortar specimens are presented in Table 2 showing the mean compressive strength and associated coefficient of variation (CoV). It is evident that the compressive strength of the bricks is approximately three times that of the mortar. The stress-strain curves of the five masonry prismatic specimens under uniaxial compression (CBM series) are presented in Figure 8 and it is shown that the mean compressive strength was 28.6MPa. Figure 9 shows the damage sustained by the masonry prisms after testing and reveals that significant damage is exhibited at load levels significantly lower than those associated with the compressive strength of the brick units. During testing, a series of vertical cracks formed and propagated along the height of the specimen, resulting in a gradual disintegration of the masonry medium of the specimens ultimately leading to a brittle form of failure once the peak load-was attained.

Table 2. Summary of material test results.

Specimen	**ID**	**Compressive Strength**		**Modulus of Elasticity**	
		Mean (MPa)	**CoV (%)**	**Mean (GPa)**	**CoV (%)**
Brick unit	CB	60	4.9	35	4.4
Mortar	CM	22	6.4	11	4.3
Masonry	CBM	28.6	38.4	21.0	21.0

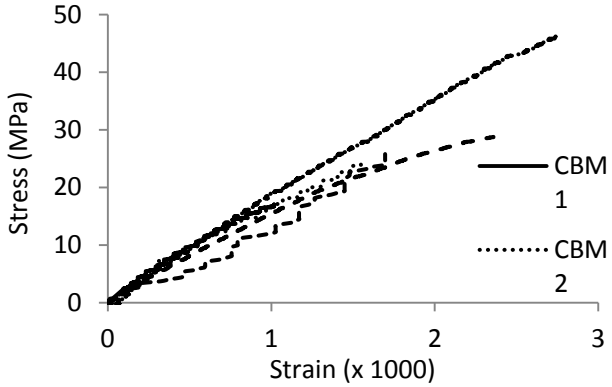

Figure 8: Compressive stress-strain curves for five brickworks under direct compression


CBM1


CBM2


CBM3


CBM4


CBM5

Figure 9: CBM specimens after failure

Shear and tensile testing of masonry couplet and triplet specimens: A summary of the results obtained from the tests carried out on couplet and triplet masonry specimens are provided in Table 3, accompanied by photos showing the state of the specimens after failure in Figure 10. It was observed that the failure of the brick/mortar (TBM series) couplets and

the brick/mortar (SBM series) triplets was exhibited along the brick/mortar interface (either in tension or shear). The mean value of the tensile strength for TBM series specimens was 0.41 MPa (CoV = 4.6%), which was approximately half of the maximum interfacial shear strength of the SBM series specimens (mean= 0.7 MPa; CoV= 19.7%). In the case of the brick/ECC (SBE series) triplets, shear failure was observed either along the ECC/brick interface or within the brick unit, with the latter attributed to the higher interfacial shear strength of the ECC/brick triplets (almost twice of that of the brick/mortar triplets (SBM series)). In all tests failure was brittle resulting in an abrupt loss of load-carrying capacity.

Table 3. Summary of tensile and shear bond strengths.

Specimen type	Mean (MPa)	COV (%)
Brick couplet	0.4	4.6
Brick/mortar triplet	0.7	19.7
Brick/ECC triplet	1.3	14.0

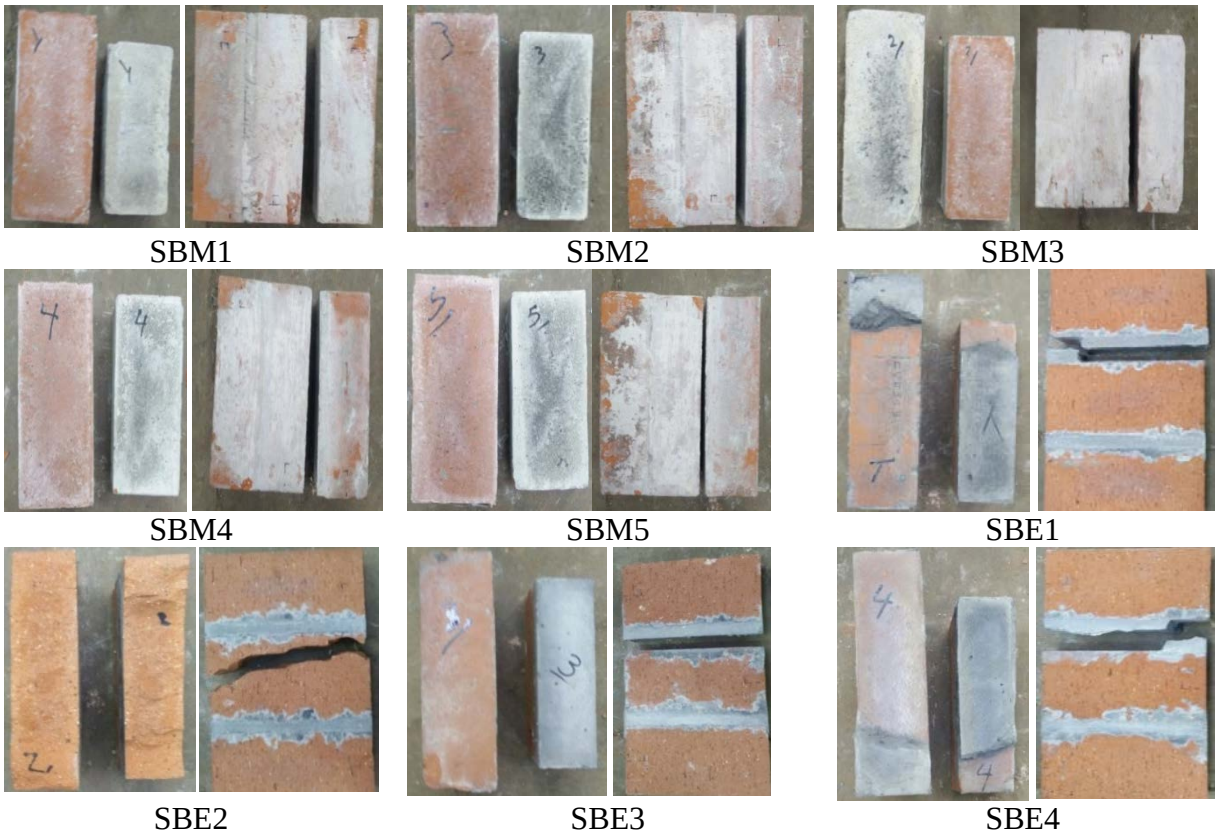

Figure 10: Failure of mortar/ECC joint, with brick/mortar (SBM) samples showing failure at the mortar/brick interface and brick/ECC (SBE) samples showing mixed failure modes.

Behaviour of ECC dog-bone specimens under uniaxial tension: The tensile stress-strain response of the ECC dog-bone specimens are presented in Figure 11. These curves consist of three different branches:

(i) an initial linear elastic (ascending) branch which starts when the loading process initiates and ends when the first cracks form;

(ii) a strain hardening branch, during which the specimen deforms with slight increase in stress. During this stage, closely-spaced fine cracks which are bridged by the PVA fibers develop, causing fluctuations to the stress-strain response; and

(iii) a steep strain softening (descending) branch, which initiates after the peak stress is attained. During this stage, one to two failure planes form as a result of fiber bridging failure.

Mean tensile stress/strain at first cracking, mean tensile strength and the corresponding strain at failure under the two different rates of loading are summarised in Table 4. The stress and strain values associated with crack initiation and the modulus of elasticity (E) are calculated from the initial stage of the loading process, whereas the tensile strength and the corresponding strain are obtained from the strain hardening branch. It is evident loading rate has a profound effect on the tensile response of the material. Under quasi-static load (ST series), the dog-bone specimens exhibited a modulus of elasticity of 15.4GPa, tensile strength of 3.8 MPa and tensile strain capacity of 3.5%. Under elevated loading rates (ET series), the dog-bone specimens exhibited higher values of modulus of elsticity (30.6 GPa) and tensile strength (5.2 MPa) but lower values of tensile strain capacity (2.2%). It should be noted that the ET series specimens exposed to higher rate of loading exhibited less number of

micocracks and larger crack widths, making the cracks more visible to the naked eye (see the comparison of the crack patterns of ST and ET series specimens at failure in Figure 12).

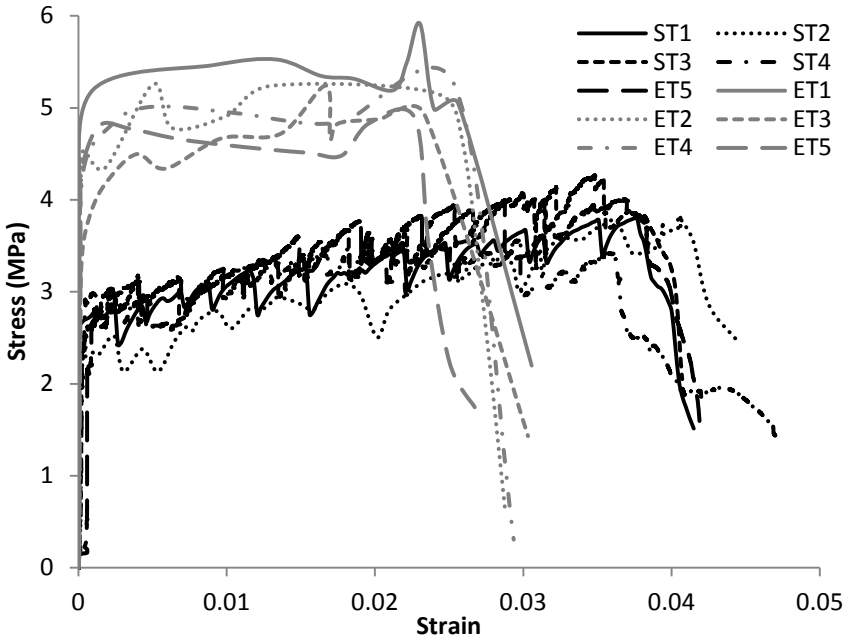

Figure 11. Tensile stress-strain curves for ST and ET series dog-bone specimens.

Table 4: Summary of tensile test results for the dog-bone specimens

ID	Loading rate (mm/min)	Stress at first cracking (MPa)	Strain at first cracking (%)	E (GPa)	Max stress (MPa)	Strain at failure (%)
ST	1	2.75	0.0180	15.4	3.85	3.5
ET	400	4.16	0.0144	30.6	5.22	2.2

a) ST series b) ET series

Figure.12. Failure crack patterns on the dog-bone specimens a) under a displacement rate of 1 mm/min and (b) under a rate of 400 mm/min.

3.2 Four-point bending tests

Behaviour of un-strengthened specimens (SN and EN series): Figure 13 shows the load-deflection curves describing the behaviour of the control (un-strengthened) masonry beam-like specimens. It is evident that the mean load-carrying capacity of the EN series specimen is approximately twice that of the SN series specimens tested under lower rate of loading. This enhancement can be largely associated with the inertia forces developing under elevated loading rates. The behaviour of all these un-strengthened specimens was characterized by a

sudden (brittle) failure, resulting in a sudden loss of load-carrying capacity, with failure occurring shortly after the development of cracking along one of the brick/mortar interfaces at the central span of the specimen (i.e. between the two locations at which the external load was applied). The results highlight the vulnerability of the masonry beams when subjected to out-of-plane forces. The state of the specimens after failure is presented in Figure 14.

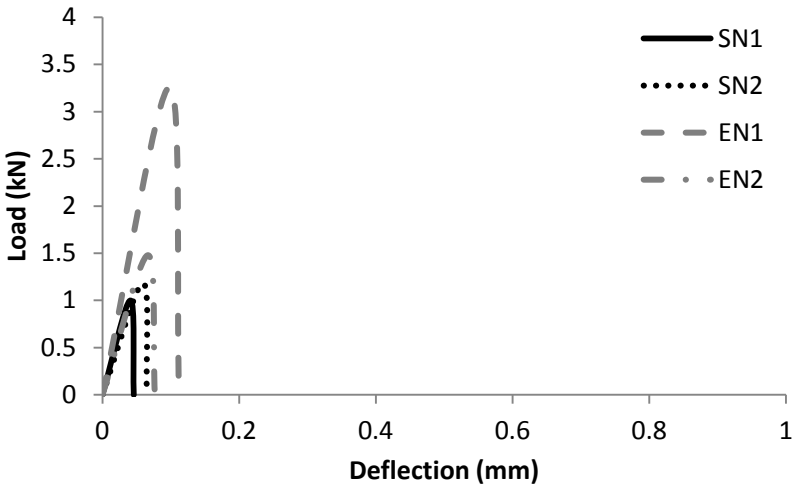

Figure 13: Load-deflection responses of the non-retrofitted masonry beams

Figure 14. Crack patterns at failure exhibited by the un-strengthened specimens when subjected to loading rates of a) 1 mm/min and (b) 200 mm/min.

Behaviour of strengthened specimens: The load-deflection curves of the ECC-retrofitted specimens subjected to 4-point bending under loading rates of 1mm/min and 200mm/min are presented in Figures 15(a) and (b), respectively. The load associated with crack initiation, the load-carrying capacity and the corresponding mid-span deflection at failure are presented in Table 5. It is evident that all ECC-strengthened specimens exhibited superior behaviour (in terms of load-carrying capacity, stiffness and ductility), when compared to that of the control (un-strengthened) specimens. From Figures 15(a) and (b), it is evident that all ECC-retrofitted specimens exhibit linear elastic behaviour until crack initiation, followed by a well-defined plateau in the load-deflection curves presented which can be associated with the tensile strain-hardening behaviour of the ECC (see Figure 11).

With reference to Figure 15(a), it is shown that both SF and SP series specimen, which strengthened with a fully and partially bonded ECC layer, exhibited values of load-carrying capacity of approximately 10 times and 8 times higher than that of the un-strengthened specimens (SN series). The fully bonded specimens (SF series) exhibited an increase of 18% in terms of the load-carrying capacity and 48% in terms of the load associated with crack-initiation, when compared to their counterparts (specimens strengthened with partially bonded ECC layers; SP series). Also, both SF and SP series specimens exhibited significantly higher out-of-plane deformation than that of the non-strengthened specimens (SN series). However, the deformability of SP beams was 69% higher than that of the SF series which can be associated with the more uniform crack formation along the central (unbonded) region (see Figure 16).

When subjected to a loading rate of 200 mm/min (see Figure 15(b)), both EF series (full bond) and EP series (partial bond) specimens exhibit a load-carrying capacity approximately 7 times and 5.5 times higher than that of the un-strengthened specimens (EN series). Furthermore, the EF series specimens exhibit load-carrying capacity and load associated with

crack-initiation 23% higher than that of their counterparts (EP series). These trends are similar to that observed in a lower rate of loading. With regards to the out-of-plane ductility, the ductility of EF and EP series specimens was approximately 13 times and 37 times higher than that of the un-strengthened specimens (EN series), with EP series specimens exhibiting a mid-span deflection at failure 183% higher than that of EF series specimens (full bond). The higher ductility exhibited by the EP specimens can be attributed to the formation of more cracks along the central (un-bonded) span (see Figure 16).

During testing, it was observed that four to five cracks at the brick/mortar interfaces over the central span of all strengthened specimens (SF, SP, EF and EP series) were visible to the naked eye before the specimens reached their ultimate limit state (ULS). As the loading progressed, these cracks were seen to extend into the compressive zone and widen as the beam continued to deflect under increasing load.

Figures 16 presents the crack patterns observed from the soffit of all ECC-retrofitted specimens after failure. In this figure, the black lines represent individual fine cracks while the red lines represent the location of the brick/mortar interfaces. All specimens reinforced with full-bond ECC layer (SF and EF series) exhibit microcracks forming locally around the joints between the bricks, regardless of the rate of loading. It is seen that these microcracks merge together, forming a larger crack that ultimately causes the ECC layer to fail, thereby resulting in the collapse of the beam specimens. From the SP and EP series specimens (partial bond), a more uniform crack formation can be seen from the central (unbonded) region regardless of the position of the brick/mortar interface, with more crack numbers seen from SP series specimens subjected to lower rate of loading. By comparing the crack patterns of full-bond and partial-bond ECC layer, it is clear that partial debonding allows the ECC layer in the unbonded region to deform more uniformly, thereby explaining the reason for the

higher ductility of the specimens strengthened with a partially-bonded ECC layer (SP and EP series).

With regards to the crack pattern across the thickness of the ECC layer, the cracks in both SF and EF series specimens (full bond) tend to originate from the cracks initiated at the brick/mortar interface, which was found to extend into the ECC layer, thereby resulting in the development of radial cracking as shown in Figure 17(a). Considering that the thickness of the ECC layer was approximately 15 mm and the maximum angle of the cracks was approximately ±45^{o} to the vertical, this gives 30 mm which is similar to the width of the cracked region on the ECC layer below each brick/mortar cracked interface. On the other hand, the cracks in SP and EP series specimens (partial bond), the cracks were more and less vertical and perpendicular to the tensile stresses acting in the ECC layer (see Figure 17(b)). The difference observed in the directionality of the cracks forming in the fully and partially ECC bonded layers of the strengthened specimens explains why the load carrying capacity of the specimens with fully bonded ECC layers is higher compared to that of the specimens with partially-bonded ECC layers.

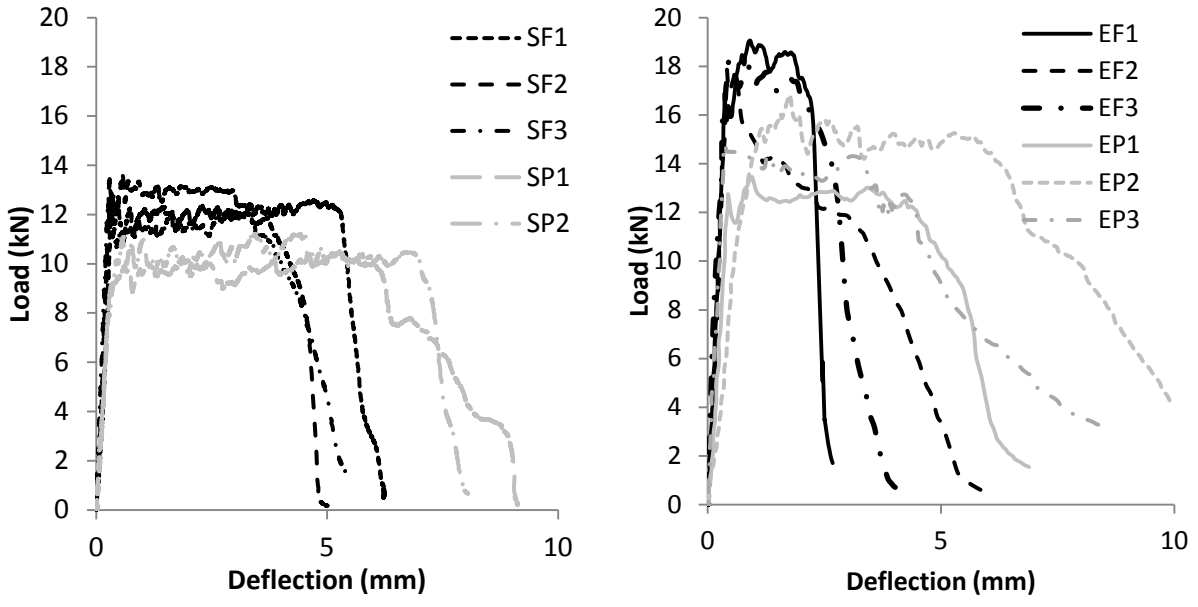

(a) (b)

Figure 15: Load-deflection responses 4-point tests specimens subjected to a loading rate of (a) 1 mm/min and (b) 200 mm/min.

Table 5: Summary of the four-point tests

Loading rate (mm/min)	ID	Average thickness (mm)	First cracking load (kN)	Average of first cracking load (kN)	Maximum load (kN)	Average of maximum load (kN)	Deflection at the maximum load (kN)	Average deflection at the max load (kN)
1	SN	-	1.1	1.2	-	-	0.05	0.06
		-	1.3		-		0.07	
	SF	16.88	13.5	12.9	13.9	12.9	3.02	3.89
		16.12	12.8		12.6		5.21	
		15.67	12.5		12.2		3.43	
	SP	15.42	9.2	8.7	11.2	10.9	7.15	6.59
		14.78	8.2		10.6		6.02	
200	EN	-	3.0	2.3	-	-	0.15	0.11
		-	1.5		-		0.08	
	EF	16.38	18.1	17.7	18.2	18.4	1.91	1.43
		16.17	17.9		17.9		0.57	
		15.57	16.9		19.1		1.82	
	EP	15.89	14.9	14.4	14.5	14.9	3.27	4.05
		15.48	12.8		13.3		3.73	
		14.93	15.5		17.0		5.16	

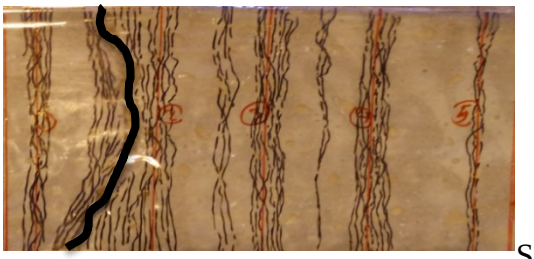

SF1

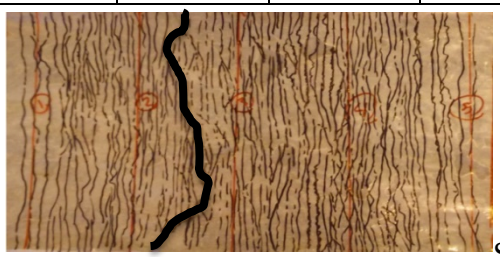

SP1

SF2

SP2

SF3

-

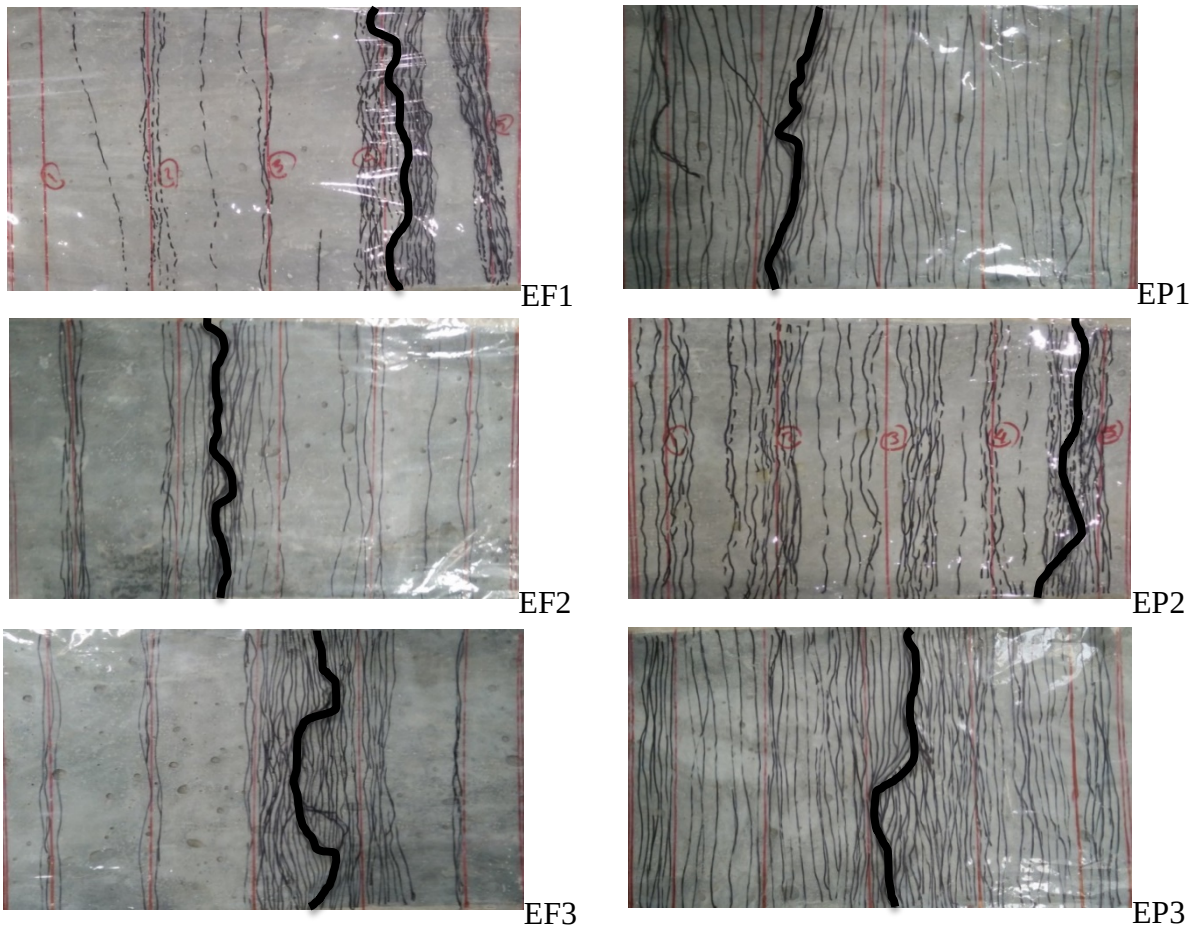

Figure 16: Failure crack pattern observed on the retrofitted ECC layer from the specimens: fully bonded series (SF and EF series), b) partially bonded series (SP, and EP series).

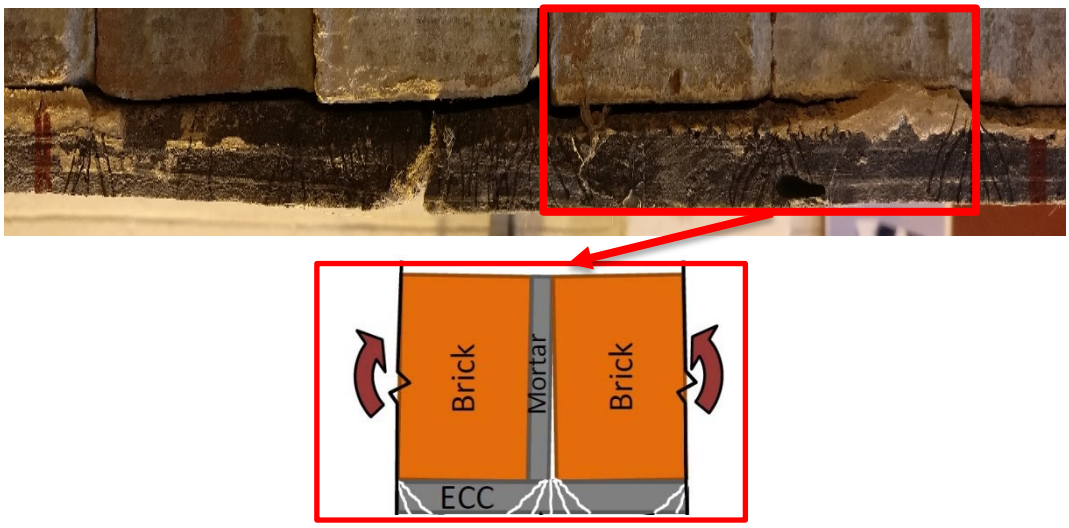

b)

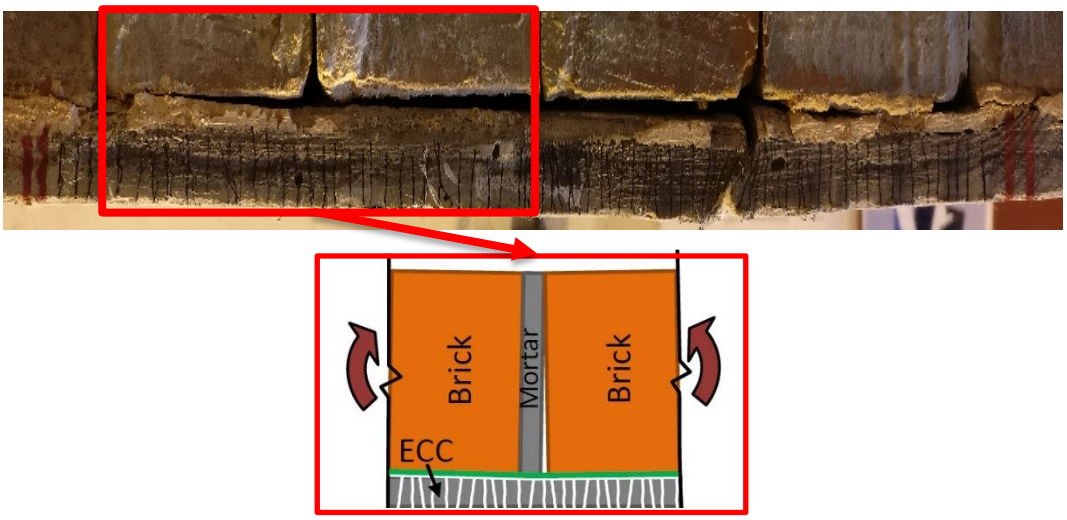

Figure 17 Comparison of the crack pattern distributed in the front face of ECC layer within the central span a) fully bonded b) partially bonded specimens.

Effect of loading rates on specimen behaviour: The test results obtained indicate that the response of the strengthened masonry specimens was influenced by the rate at which the imposed load was applied (1 mm/min or 200 mm/min). Increasing the loading rate from 1 mm/min to 200 mm/min caused SF and EF series specimens (full bond) to exhibit a 37% and 42% increase in the level of loading associated with crack initiation and load carrying capacity, respectively. When subjected to elevated rate of loading (200mm/min), EF series specimens (full bond) still exhibited an essentially elastoplastic strain-hardening behavior after crack initiation, although the midspan deflection at failure was ~63% less than that exhibited by the same specimens under lower rate of loading (1mm/min) (SF series).

In the case of the specimens with partially bonded ECC layers, increasing the rate of loading has caused the EP series specimens to exhibit the load at crack initiation and the peak load, respectively, 65% and 36% higher than that of SP series specimens (under loading rate of

1mm/min). However, the mid-span deflection of EP series specimens at failure was 40% less than that of the SP specimens. The enhancement in load-carrying capacity and reduction in deformability under increasing loading rates can be attributed to the strain-rate dependency of the ECC, as confirmed by the results of the ECC dog-bone specimens under increasing rates of tensile loading (see Figure 11).

Overall, it is interesting to highlight that the reduction of the deformability exhibited by the strengthened specimens with a partially bonded ECC layer under increasing loading rates (EP series) is 58% lower than that of the fully bonded specimens (EF series). This fact highlights the advantage of using partially bonded ECC layers over the range of the rate of loading investigated herein.

With reference to Figure 16, it is evident that the crack number is affected by the rate of loading, with both SF and SP series specimens consistently showing less number of cracks to those tested under higher rate of loading (EF and EP series). This can also be associated with the strain rate dependent characteristics of the ECC as was observed earlier in the dog-bone ECC specimens when subjected to different rates of loading. The development of fewer cracks along the ECC layers of the strengthened specimens under increasing loading rates provides the evidence to as why EF and EP specimens exhibited less ductility.

4. Numerical modelling of the retrofitted masonry beam-like specimens

Based on the results obtained from the tests carried out a series of preliminary finite element models were developed to predict the behaviour of the masonry beam-like specimens investigated experimentally under static loading. A commercial nonlinear finite element analysis (NLFEA) software (ADINA, 2014) is used which incorporates a number of

513 constitutive models capable of realistically describing the behaviour of the relevant materials
514 and interfaces. It also employs an iterative solution procedure, based on the Newton-Raphson
515 method, allowing it to account for the stress redistributions exhibited due to the exhibited
516 cracking. The problem at hand is a 2-dimensional plain-strain model. 4-noded 2-D finite
517 elements are employed to model the bricks, the mortar and the ECC layers. The material
518 properties of the masonry unit and the mortar are described using the concrete material
519 model. The ECC is modelled using a simple multi-linear material model. Elastic steel
520 elements are used to represent the plates located at the supports and at the point where the
521 load is exerted. These elements are used to avoid the development of high stress
522 concentrations that can result in the formation of localised cracking that may cause the pre-
523 mature failure. Table 6 shows the summary of the values adopted for the various parameters
524 required for defining the material and interface models presently adopted.

525

526

527

Table 6. Main parameters used to define the various material and interface models employed herein.

Property	**Symbol**	**Value**	**Source**
Brick			
Elastic modulus	E_{brick}	35GPa	CB test series
Compression strength	fc_{brick}	60MPa	
Tensile strength	ft_{brick}	6 MPa*	
Mortar			
Elastic modulus	E_{mortar}	11GPa	CM test series
Compression strength	Fc_{mortar}	22MPa	
Tensile strength	Ft_{mortar}	2.2 MPa*	
ECC			
Elastic modulus	E_{ECC}	15.4 GPa	ST test series
Compression strength	fc_{ECC}	30MPa	
Stress at first crack	$\sigma_{First\ crack}$	2.75 MPa	
Strain at first crack	$\varepsilon_{first\ crack}$	0.00018	

Peak stress	σ_{max}	3.85	
Strain at peak stress	ε_{max}	0.035	
Strain at failure	$\varepsilon_{failure}$	0.04	
Brick-mortar interface			
Shear strength	V_{BM}	0.7Mpa	SBM test series
Shear modulus	G_{BM}	16GPa†	
Tensile strength	T_{BM}	0.4MPa	SBE test seres
Brick-mortar interface			
Shear strength	V_{BM}	1.3MPa	TBM tests series
Shear modulus	G_{BM}	50GPa†	

* determined based on 10% of the measured compressive strength

† measured during the experimental tests

4.1 Modelling approach

Figure 18a presents the finite element (FE) model adopted for representing the non-retrofitted masonry specimen (SN series). Due to the symmetry characterising the problem at hand only half of the specimen was simulated. The FE model comprises of five bricks and five mortar layers between the bricks. The size of the bricks was 102mm x 65mm. Each brick was modelled by a 6 x 10 FE mesh. The thickness of mortar layer (joint) was 10mm except in the case of the layer at the mid-span of the specimen which had a thickness of 5mm (due to the symmetry conditions of specimen only half of the thickness of the middle mortar joint was modelled). All mortar layers were modelled by a 1x10 FE mesh. Cohesive elements were defined at the interface between the brick and the mortar layer based on the results presented in Table 6. All nodes located on the face of the model at its right end (essentially representing the mid-span region of the specimen) were restricted from moving axially. The specimen was supported on a steel plate which was allowed to move axially and rotate along its mid-span (forming a roller). A concentrated load (see figure 18a) was applied monotonically to failure in the form of displacement increments.

The same model was used to investigate the behaviour of the strengthened specimens (see Figure 18.b and c). A 15mm think ECC layer was added to the lower face of the masonry beam and was modelled using a 4x100 mesh of 4-noded 2D plain-strain elements. The ECC layer was either considered fully bonded to the masonry surface or was assumed un-bonded in the middle third span of the specimen (see the blue line in Figure 18c) by introducing a contact surface between the ECC layer and the masonry specimen.

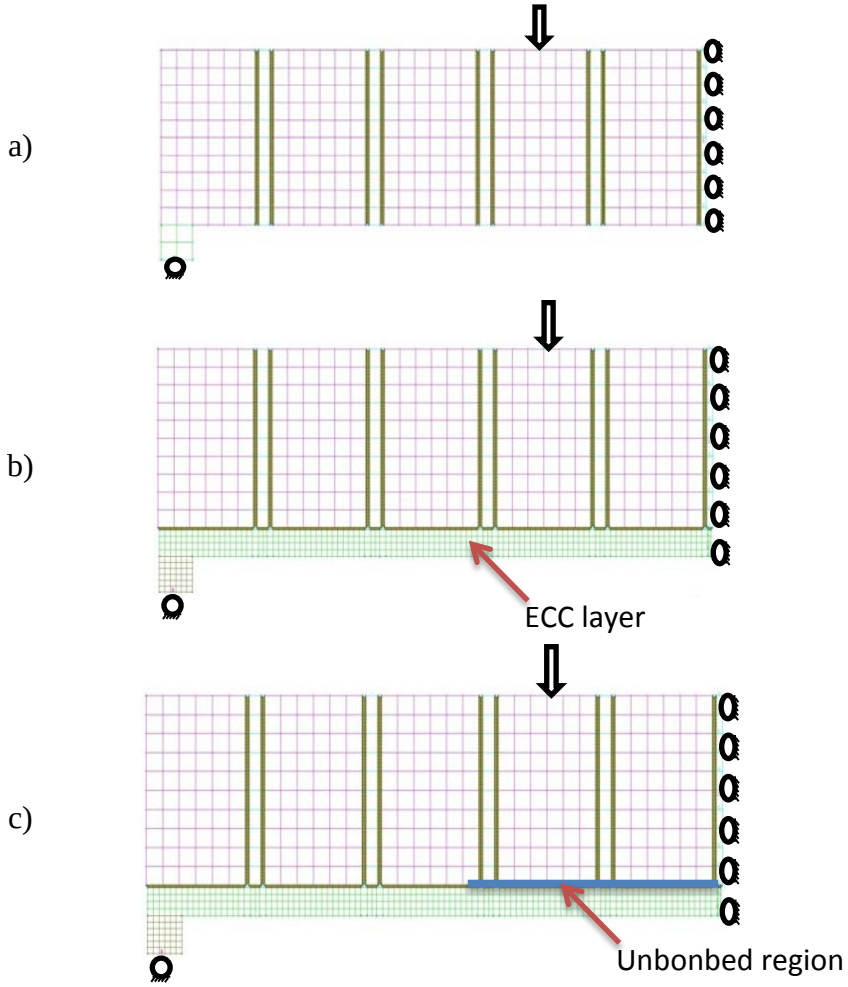

Figure 18 a) FE model developed for the a) SN specimens, b) FE model developed for the SF specimens c) FE model developed for the SP specimens

4.2 Result of simulation and discussion:

560 The predictions obtained from the un-strengthened specimens (SN-series) concerning the
561 load–defection curves (see Figure 19.a) as well as the mode of failure (see Figure 20a) exhibit
562 similar trends with their experimentally established counterparts. However, the numerically
563 predicted load-bearing capacity is higher than that established experimentally. This difference
564 can be attributed to the variation of the material properties that often characterise masonry or
565 to the effect of imperfections associated with the manufacturing process of the subject
566 specimen that can have a significant effect on the behaviour of specimens characterised by
567 low load-carrying capacities and exhibiting brittle modes of failure as is the case for the un-
568 strengthened specimens presently considered. The mode of failure predicted numerically was
569 associated with failure along the cohesive interface (defined between the mortar and the
570 brick) which was in line with what was observed experimentally (Figure 20a).
571
572 The predictions obtained from the model describing the behaviour of the strengthened
573 specimens with a fully bonded ECC layer (SF series) are presented in Figure 19b in the form
574 of curves expressing the variation of the applied load with the mid-span defection. The
575 predicted response is in generally good agreement with that established experimentally. The
576 load carrying capacity established experimentally is higher than that predicted numerically.
577 This can be attributed to the variation of the properties and thickness of the ECC layer in the
578 actual specimens (the ECC layer was 1-2 mm thicker in the region of the mortar joints).
579 Furthermore, the numerical predictions tend to underestimate the ductility of the specimens
580 established experimentally. This can be attributed to the fact that during testing, de-bonding
581 occurred locally (at a critical region) between one brick and the ECC layer –along the
582 specimen span between the two points at which the loads are applied (approximately the
583 middle third of the span, see Figure 17b). This de-bonding enables the development of
584 cracking within the ECC layer ultimately resulting in local failure (see Fig 15). However, this

process is not adequately simulated in the FE model presently employed. Failure of the interface between the brick and mortar is predicted, which is in agreement with the failure mode observed during testing, which is then followed by the development of cracking in the ECC layer ultimately resulting in failure of the ECC layer. The distribution of strain within the FE model (see Figure 20b) reveals the development of high stress concentrations near the mortar joints which is compatible with crack patterns observed during testing. However, it appears that the ECC layer fails under lower levels of deformation compared to those achieved by the actual specimens.

Model represents the partially bonded specimens: The numerical predictions describing the behaviour of the strengthened specimens with a partially bonded ECC layer (SP series) are presented in Figure 19c in the form of curves expressing the variation of the applied load with the mid-span defection. The numerical predictions are in good agreement with their experimentally established counterparts. Once again the numerical model tends to underestimate the load-carrying capacity of the specimens for the same reasons discussed in the case of the specimens with fully bonded ECC layers. However, in terms of ductility the experimental and numerical predictions correlate closely. Failure in the model initially occurs in the cohesive interface between the brick and mortar, this is followed by the development of distributed cracking along the un-bonded ECC layer ultimately resulting in the failure of the ECC layer and the collapse of the specimen (see Figure 20c). This is in line with the cracking process observed during the test.

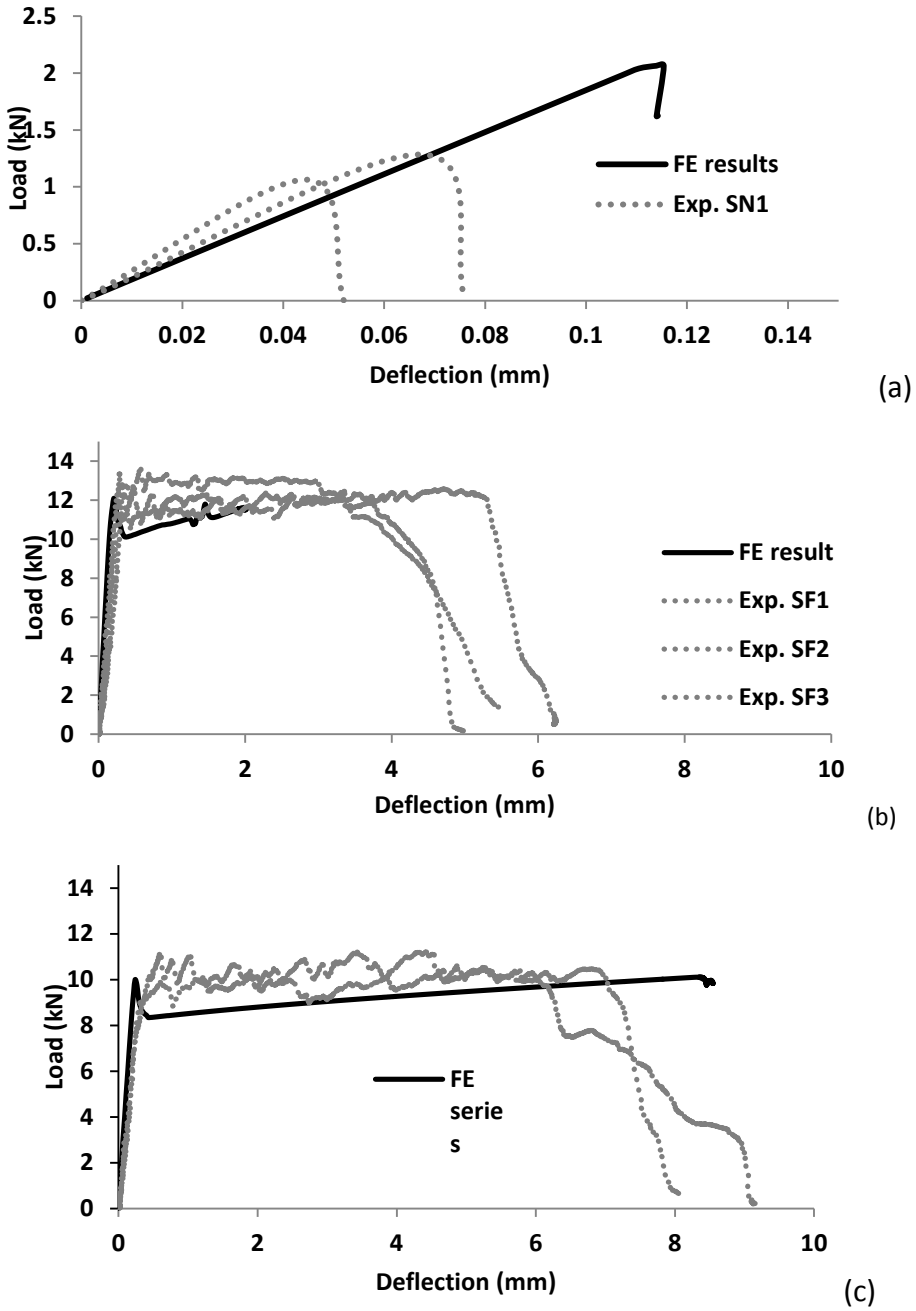

606 Figure 19. Comparison of numerically and experimentally established load-deflection curves describing the
607 behaviour of a) the un-strengthened specimens (SN-series), b) the specimens strengthened with a
608 fully bonded EEC layer (SF-series) and c) the specimens strengthened with a partially-bonded
609 EEC layer (SP-series)
610

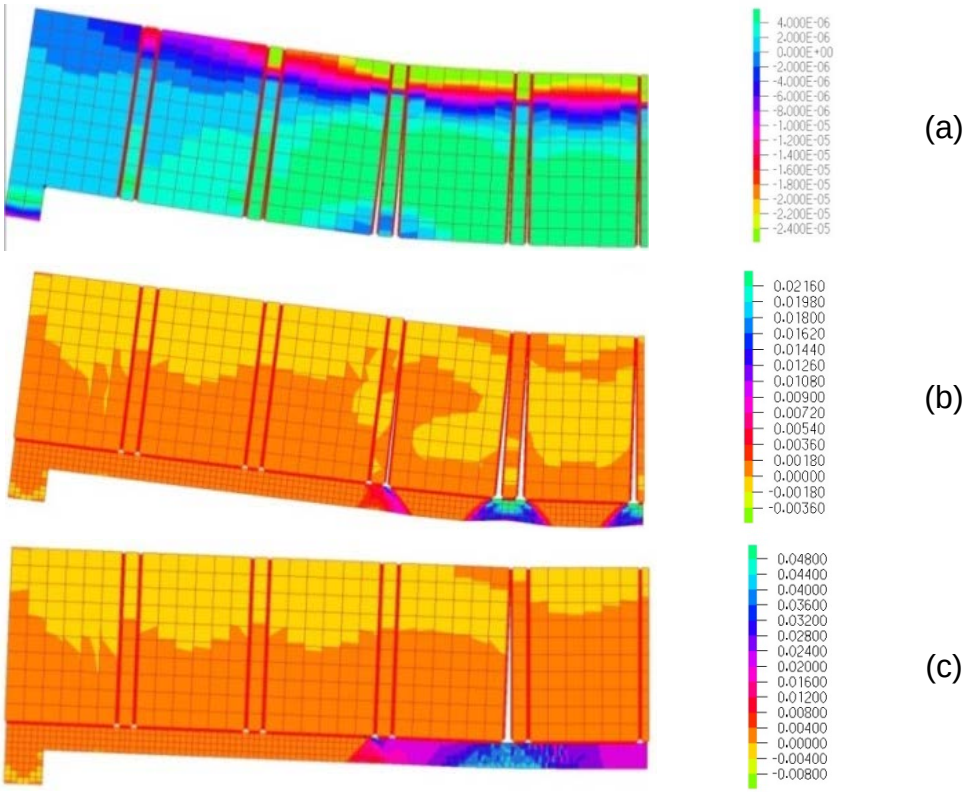

Figure 20. Predicted strain distribution at failure for the case of a) the un-strengthened specimens (SN-series), b) the specimens strengthened with a fully bonded EEC layer (SF-series) and c) the specimens strengthened with a partially-bonded EEC layer (SP-series)

5. Conclusions

Based on the experimental study carried out in this paper, the following conclusions can be drawn from the present study:

- Strengthening of the masonry walls with an ECC layer can significantly improve their performance in terms of load-carrying capacity, stiffness, deformability and ductility.

- The bond between the ECC layer and the masonry specimens is an important parameter that affects the behaviour of the strengthened masonry beams. The ductility of the masonry beams strengthened with a partially-bonded ECC layer when subjected to low or

627 elevated loading rates is approximately 1.5 to 2 times higher than that of the specimens
628 with a fully bonded layer.
629
630 • The specimens strengthened with a partially bonded layer of ECC exhibit ductile
631 behaviour due to the multiple cracks forming primarily within the ECC layer which was
632 unbonded from the masonry surface. The microcracks developing in the ECC layer were
633 vertical and perpendicular to the tensile stresses developing along the ECC layer,
634 indicating negligible influence from the masonry substrate. The uniform crack patterns
635 from the partially bonded ECC specimens indicate better utilization of the ECC layer,
636 thereby allowing the specimens to exhibit larger deformations.
637
638 • The specimens strengthened with a fully bonded layer of ECC developed multiple cracks
639 clustered nearby the brick/mortar joints. Most of the cracks were at an angle due to the
640 interaction exhibited between the ECC layer and the masonry resulting in an increase in
641 the tensile strength of the ECC layer and consequently the load-carrying capacity of the
642 strengthened specimen compared to that exhibited by the specimens with partially bonded
643 layers.
644
645 • Beams with fully bonded ECC layer exhibited a 66% increase in the load associated with
646 crack initiation and a 33% increase in load carrying capacity, when subjected to elevated
647 loading rates, as compared to their counterparts under equivalent static loading. The
648 specimens with partially bonded ECC layers exhibited a 36% increase in the load at first
649 cracking and a 42% increase in load-carrying capacity, when compared to their
650 counterparts tested under lower rates of loading. The higher load carrying capacity of the
651 specimens under increasing loading rates is primarily associated with the strain rate

sensitivity of the ECC, and to a lesser extent, the increasing inertia effect with increasing rate of loading.

- The masonry beam specimens with fully and partially bonded ECC layers exhibited, respectively, a 66% and 35% reduction in deflection capacity when subjected to increased rate of loading, as compared to their counterparts tested under low (static) rate of loading. This reduction is associated with the strain rate dependent characteristics of the ECC, which was confirmed through simple uniaxial tensile tests on dog-bone shaped specimens. SSpecimens with a partially bonded ECC layer exhibited less reduction of displacement capacity, with the absolute value approximately twice that of the specimens with a fully bonded ECC layer. This reduction in displacement capacity was found to be attributed to the localized crack formation at the brick-mortar interface(s).

- The Finite element models developed for predicting the response of the ECC-retrofitted masonry beams investigated experimentally can realistically predict the behaviour observed during testing confirming the main findings of the experimental study concerning the enhancement achieved in specimen behaviour through the use of the fully and partially bonded ECC layers.

6. Acknowledgements

The authors wish to acknowledge the support of Kuraray Japan for providing the PVA fibres and BASF UK for providing the admixtures and the financial support by the School of Energy, Geoscience, Infrastructure and Society at Heriot-Watt University.

7. References

[1].Abrams, D.P., R. Angel, and J. Uzarski, *Out-of-plane strength of unreinforced masonry infill panels.* Earthquake spectra, 1996. 12(4): p. 825-844.

[2].Mehrabi, A.B., Benson, S., Schuller, M., Noland, J., *Experimental evaluation of masonry-infilled RC frames.* Journal of Structural Engineering, 1996. 122(3): p. 228-237.

[3].Murty, C. and S.K. Jain. *Beneficial influence of masonry infill walls on seismic performance of RC frame buildings. in Proceedings of the 12th World Conference on Earthquake Engineering, Auckland, New Zealand, Paper. 2000.*

[4].Cavaleri, L., M. Fossetti, and M. Papia, *Modeling of out-of-plane behavior of masonry walls.* Journal of structural engineering, 2009. 135(12): p. 1522-1532.

[5].Griffith, M. and J. Vaculik, *Out-of-plane flexural strength of unreinforced clay brick masonry walls.* TMS Journal, 2007. 25(1): p. 53-68.

[6].Bruneau, M., *State-of-the-art report on seismic performance of unreinforced masonry buildings.* Journal of Structural Engineering, 1994. 120(1): p. 230-251.

[7] FEMA 306 , Evaluation of earthquake damaged concrete and masonry wall buildings, 1998

[8] EC8, Design of structures for earthquake resistance, 1998

[9] Tiedeman, H., *A statistical evaluation of the importance of non-structural damage to buildings. In Proc., 7th World Conf. on Earthquake Engrg* 1980*: (pp. 617-624).*

[10].Hutchison, D., P. Yong, and G. McKenzie, *Laboratory testing of a variety of strengthening solutions for brick masonry wall panels, 8th WCEE.* San Francisco, USA, 1984: p. 575-582.

[11].Karantoni, F.V. and M.N. Fardis, *Effectiveness of seismic strengthening techniques for masonry buildings.* Journal of Structural Engineering, 1992. 118(7): p. 1884-1902.

[12].Abrams, D. and J. Lynch. *Flexural behavior of retrofitted masonry piers*. in *KEERC-MAE Joint Seminar on Risk Mitigation for Regions of Moderate Seismicity*. 2001.

[13].Sheppard, P. and S. Tercelj. *The effect of repair and strengthening methods for masonry walls*. in *7th World Conference on Earthquake Engineering*. 1980.

[14].ElGawady, M., P. Lestuzzi, and M. Badoux. *A review of conventional seismic retrofitting techniques for URM*. in *13th international brick and block masonry conference*. 2004. Citeseer.

[15].Taghdi, M., *Seismic retrofit of low-rise masonry and concrete walls by steel strips*. 1998: University of Ottawa (Canada).

[16].Carney, P. and J.J. Myers. *Shear and flexural strengthening of masonry infill walls with FRP for extreme out-of-plane loading*. in *Proceedings of the Architectural Engineering Institute 2003 Annual Meeting*. 2003.

[17].Ward, S.P., *Retrofitting existing masonry buildings to resist explosions.* Journal of performance of constructed facilities, 2004. 18(2): p. 95-99.

[18].Mosallam, A.S., *Out-of-plane flexural behavior of unreinforced red brick walls strengthened with FRP composites.* Composites Part B: Engineering, 2007. 38(5): p. 559-574.

[19].Amiraslanzadeh, R., Ikemoto, T., Miyajima, M.,Fallahi, A., A Com*parative Study on Seismic Retrofitting Methods for Unreinforced Masonry Brick Walls.*

[20].Li, V.C., *On engineered cementitious composites (ECC).* Journal of advanced concrete technology, 2003. 1(3): p. 215-230.

[21].Yang, E. and V.C. Li. *Rate dependence in engineered cementitious composites*. in *International RILEM Workshop on High Performance Fiber Reinforced Cementitious Composites in Structural Applications*. 2006. RILEM Publications SARL.

724 [22].Mechtcherine, V., Silva, F., Butler, M., Zhu, D., Mobasher, B., Gao, S., Mäder, E.,
725 *Behaviour of strain-hardening cement-based composites under high strain rates.*
726 Journal of Advanced Concrete Technology, 2011. 9(1): p. 51-62.

727 [23]. Davidson, J.S., Fisher, J., Hammons, M., Porter, J., Dinan, R., Failure *mechanisms of*
728 *polymer-reinforced concrete masonry walls subjected to blast.* Journal of Structural
729 Engineering, 2005.

730 [24]. Dehghani, A., G. Fischer, and F.N. Alahi, *Strengthening masonry infill panels using*
731 *engineered cementitious composites.* Materials and Structures, 2015. 48(1-2): p. 185-
732 204.
733 [25]. Kyriakides, M., M. Hendriks, and S. Billington, *Simulation of unreinforced masonry*
734 *beams retrofitted with engineered cementitious composites in flexure.* Journal of
735 Materials in Civil Engineering, 2012. 24(5): p. 506-515.

736 [26].Li, V.C., Horii, H., Kabele, P., Kanda, T., Lim, Y., R*epair and retrofit with engineered*
737 *cementitious composites.* Engineering Fracture Mechanics, 2000. 65(2): p. 317-334.

738 [27]. BS EN 771-1, 'Specification for masonry units. Clay masonry units'. 2011

739 [28]. ASTM C67, 'Standard test method for sampling and testing brick and structural clay
740 tile' 2014

741 [29]. BS EN 197-1, 'Cement. Composition, specification and conformity criteria for common
742 cements'. 2011

743 [30]. ASTM C952-12, 'Standard test methods for bond strength of mortar to masonry units'.
744 2012

745 [31]. BS EN 1052-3, 'Methods of thest for masonry. Determination of initial shear strength'.
746 2002

747 [32]. ASTM C1314-14, 'Standard test method for compressive strength of masonry prisms'.
748 2014

749 [33]. ASTM C1552-15, 'Standard practice for capping concrete masonry units, related units
750 and masonry prisms for compression tests'. 2015

751 [34]. JSCE, 'Recommendation for design and construction of high performance fibre
752 reinforced cement composites with multiple fine cracks (HPFRCC)'. 2008